Comparisons of H_∞ control and generalized predictive control for a laser scanner system

A W Ordys[1]*, **J Stoustrup**[2] and **I Smillie**[3]
[1]Industrial Control Centre, University of Strathclyde, Glasgow, Scotland, UK
[2]Department of Control Engineering, Aalborg University, Aalborg, Denmark
[3]Barr and Stroud Limited, Glasgow, Scotland, UK

Abstract: This paper describes tests performed on a laser scanner system to assess the feasibility of H_∞ control and generalized predictive control design techniques in achieving a required performance in a trajectory following problem. The two methods are compared with respect to achieved scan times, tracking errors and overshooting. The results are illustrated on a simulation example.

Keywords: modelling and simulation, predictive control, H_∞ control, systems with friction

NOTATION

a_1, a_2, b_1, b_2	constants in the pole-zero compensator equation
$\mathbf{A}, \mathbf{B}, \mathbf{C}, \mathbf{D}$	matrices in the state-space representation of the system
$\tilde{\mathbf{A}}, \tilde{\mathbf{B}}, \tilde{\mathbf{C}}$	matrices in the extended state-space formulation in the GPC formulation of the problem
c_g	cogging
$\mathbf{G}(s)$	transfer function of the plant, the corresponding state-space representation consists of the matrices $\mathbf{A}, \mathbf{B}, \mathbf{C}, \mathbf{D}$
$\mathbf{G}_{N_1,N_2}, \mathbf{G}_{N_1,N_2,N_u}$	matrices in the prediction equation
i_m	motor current (A)
J	performance index in the GPC formulation of the problem
J_1, J_2	motor and the mirror moments of inertia in the scanner dynamic equation (kg m^2)
$\mathbf{K}(s)$	transfer function of the controller
K_b	constant in the voltage equation
K_t	constant in the electric torque equation
$K_1(s)$	transfer function of the feedforward controller
$K_2(s)$	transfer function of the feedback controller
L, R	constants in the motor current equation
N_1, N_2, N_u	horizons in the GPC formulation of the problem
p_f	profile
r_t	scanner reference signal (rad)
T_e	electric torque of the motor (N m)
T_o	output torque of the motor (N m)
T_t	torsional link between the mirror and the motor (N m)
u_t	control signal, current demand (A)
$\Delta\boldsymbol{u}$	control increment in the GPC formulation of the problem
V_m	motor command signal from the Power_Amplifier (V)
ΔV	voltage supplied to the scanner motor (V)
w_1, w_2, w_3	disturbance signals in the H_∞ formulation of the problem
$\mathbf{W}(s)$	weighting transfer function in the H_∞ formulation of the problem, the corresponding state-space representation consists of the matrices $\mathbf{A}_W, \mathbf{B}_W, \mathbf{C}_W, \mathbf{D}_W$
$\boldsymbol{x}$	state of the scanner system
$\boldsymbol{x}_W$	state of the reference generator
y_t	scanner output signal, the mirror position measured by the Position_Sensor (rad)
$\boldsymbol{Y}_{t,N_1,N_2}$	vector of future outputs of the system in the GPC formulation

The MS was received on 8 October 1999 and was accepted after revision for publication on 25 January 2000.
* *Corresponding author: Industrial Control Centre, Department of Electronic and Electrical Engineering, University of Strathclyde, Graham Hills Building, 50 George Street, Glasgow G1 1QE, Scotland, UK.*

z_1, z_2	output signals in the H_∞ formulation of the problem
θ_1	motor position (rad)
θ_2	mirror position (rad)
λ	parameter in the H_∞ formulation of the problem, also a parameter in GPC formulation of the problem
ρ	parameter in the H_∞ formulation of the problem
$\mathbf{\Phi}_{N_1,N_2}$	matrix in the prediction equation
χ	extended state of the scanner

1 INTRODUCTION

1.1 Description of the scanner

Performance improvements in scanning devices offer the opportunity to build cost-effective scanning systems that are simple, fast, accurate, compact and capable of applications previously in the domain of other technologies. Traditional applications exist in the industrial, commercial, medical, military, communications and entertainment market. Newer applications are being introduced (see reference [**1**]).

The function of the frame scan system is to sweep an optical beam across a focal plane array detector such that scene information can be gathered. This motion of the beam must meet system level interface requirements with regard to aperture, speed and accuracy.

A galvanometric scanner is a form of electric motor in which the armature is restrained so that it can rotate only through angles of $\pm 30^\circ$ or less. A plane mirror with its surface parallel to the axis of rotation is rigidly mounted on the projecting shaft of the armature. The armature, mirror and mirror mount are collectively referred to as the rotor.

For speed and accuracy the scanning system ought to possess high torque and high torque–inertia ratio. To meet these requirements, the scanning device designer must address the intertwined design and construction of the torque motor, mirror, suspension and position encoder.

The current moving-magnet scanners are built with rare-earth magnets that generate a high torque without demagnetization. They are designed for rigidity and structural integrity so that the scanner will not self-destruct from fatigue. They also have the ability to dissipate heat generated in the stator coil so that the unit will not burn out. Thus, three critical design elements for a modern scanner are the following:

(a) an accurate, thermally stable mirror position detector;
(b) a rotor with highly rigid armature, bearings, mirror and mirror mount;
(c) a stator drive coil with good thermal conductivity.

1.2 The control requirements specification

The operation of the scanner consists of oscillatory movements of the mirror, during which the optical information is gathered through the use of a laser beam. For the purpose of this study, the optical part of the system is not considered. This study concerns only the control of the rotation of the mirror. The control system requirements can be illustrated as in Fig. 1. This figure presents a typical reference signal for the scanner system, the output from the scanner system, i.e. the mirror position and the position error. The scan period can be read directly from the graph as 0.02 s (the frequency is 50 Hz). The linear scan time is defined as a fragment of the scan period in which the tracking error lies within certain boundaries. If, for example, the boundaries of tracking error (0.0005, 0.0025) (rad) are considered (note that a steady state offset is accounted for), then the linear scan time is as depicted in Fig. 1. The purpose of the control system is then to make the mirror angular position follow the reference signal as tightly as possible, especially within the linear scan time. Therefore, the position error is to be minimized. For this particular study, the following parameters determine the performance of the system.

Scan angle. This determines the maximum field of view in object space. For contemporary designs the resulting mirror motion for the frame scanner falls in the range of 5–9° of displacement. An additional margin of 3° is required for imaging calibration targets (thermal references) on to the array sensor. Thus, the rotational range of the frame scanner must provide 12° of mechanical motion. The scan angle can be read from the top part of Fig. 1 as changing from -0.11 rad (-6.3°) to 0.11 rad (6.3°).

Scan rate. In order to be compatible with existing display standards, it is preferred that the frame scanner operates at the frequency of 50 Hz (60 Hz in the USA).

Scan efficiency. This is directly related to the amount of time spent collecting scene information. Therefore, the scan efficiency is defined as the ratio of linear scan time to the scan period. In Fig. 1 the linear scan time can be read as 0.0146 s. When this is divided by the scan period of 0.02 s, it gives the scan efficiency of 73 per cent. For the shape of the reference signal defined in Fig. 1 the maximum achievable scan efficiency would be 85 per cent. Typical requirements for a minimum scan efficiency is 80 per cent in order to achieve the current system level performance specifications.

Velocity non-linearity. Linear operation of the frame scanner is critical to maintaining the image quality. By reducing the scan velocity non-linearity to the level of 0.5 per cent a special non-linearity compensation is no longer required. This can eliminate the dither noise in the detectors and therefore improve significantly the

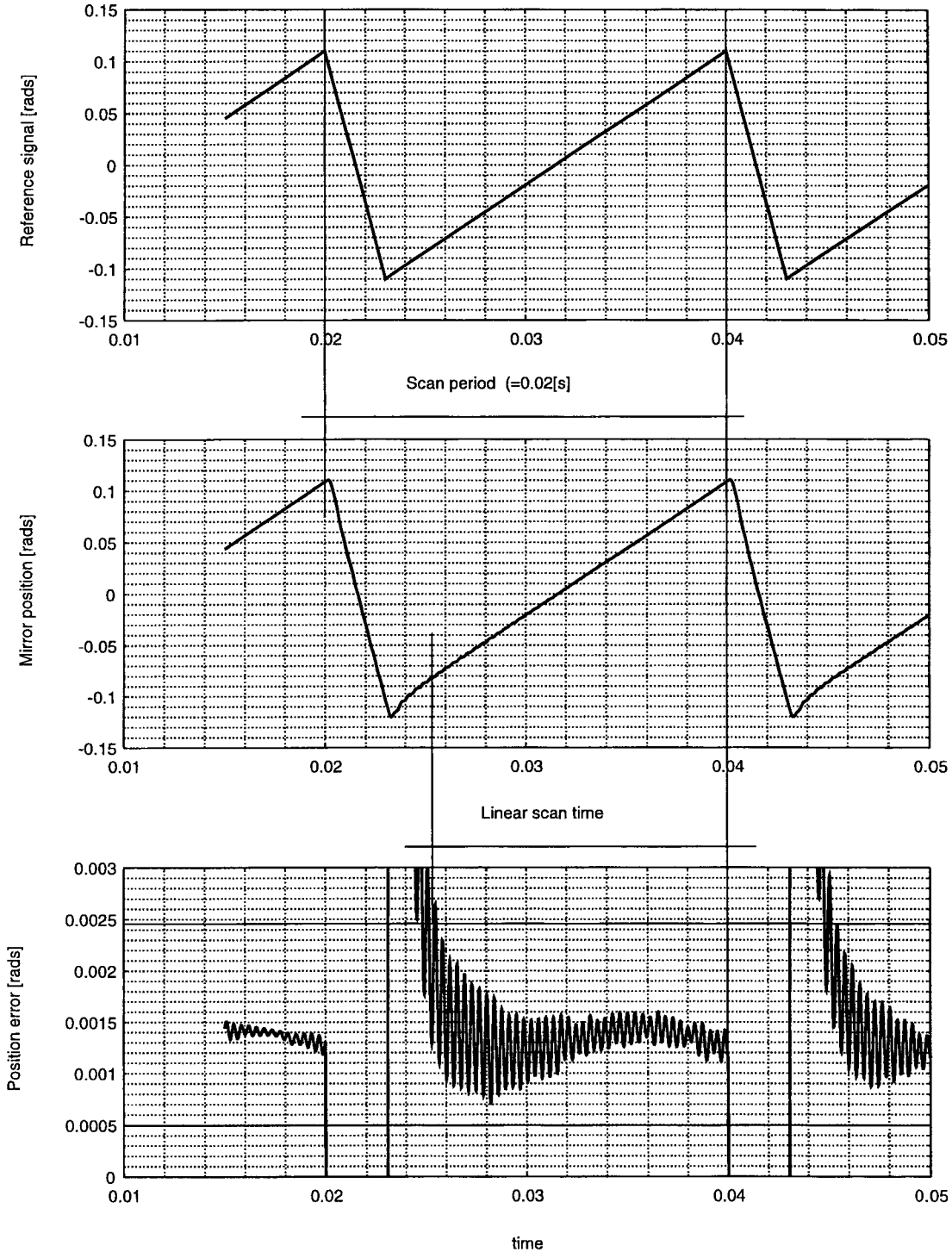

Fig. 1 The scanner reference signal and control requirements

quality of images. The velocity non-linearity is not depicted in Fig. 1 as it has not been analysed in this study.

1.3 Motivation for advanced control strategies

The overall block diagram of the scanner system is presented in Fig. 2. The controller currently implemented is a first-order pole-zero compensator. The controller provides a reasonable performance of the system but the tracking error is very close to allowable limits and the scan efficiency is only around 73 per cent. It is hoped that the advanced control techniques will improve the overall performance. When considering candidate advanced controllers the following factors were taken into consideration:

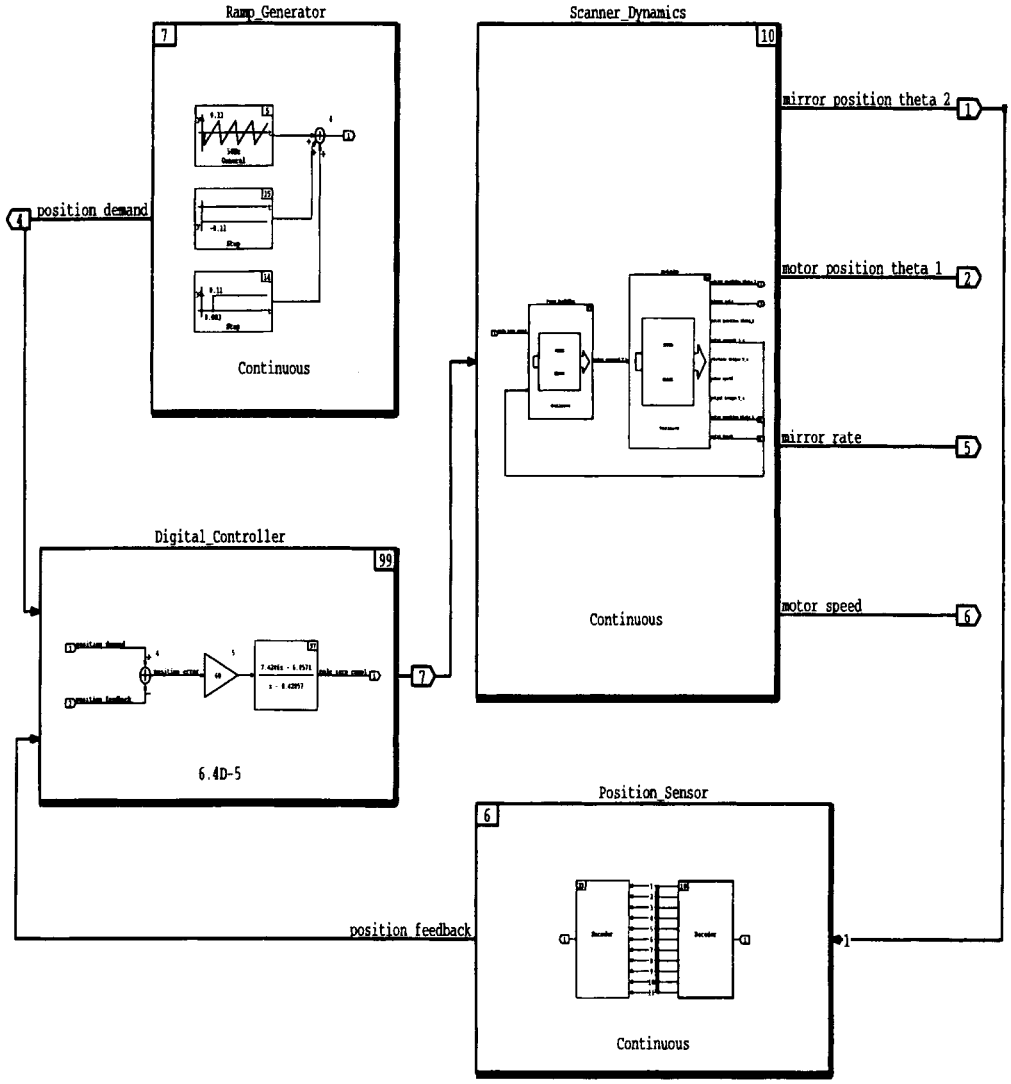

Fig. 2 The overall block diagram of the scanner system, MATRIXx representation

1. The scanner system is strongly non-linear. Moreover, the available model, although very detailed, is only a medium-fidelity approximation of the real scanner system. Therefore the control strategy must be robust with respect to non-linearities and unmodelled effects. H_∞ could therefore be a promising strategy [**2**].
2. The reference signal for the scanner system is known and will not change in the future. Therefore, if this knowledge is included into the controller design, an improvement in performance can be expected. This suggests immediately model-based predictive control. Moreover, the predictive control has been applied successfully to similar types of problem (J. Richalet, ADERSA, Paris, 1996, personal communication).

2 Modelling the scanner

2.1 Main parts of the scanner system

A detailed non-linear model of the laser scanner has been developed at Barr and Stroud Limited. This model cannot be presented due to its confidentiality. Therefore, only the general structure of the model is outlined in this paper. In particular, the non-linear effects of profile and cogging and the friction model are deliberately omitted. However, the reader is referred to references [**3**] and [**4**] for the general principles of modelling mechanical systems with friction. Figure 2 shows the overall block diagram of the scanner system. The system consists of the following:

(a) the reference signal generator (Ramp_Generator), where the reference signal is as depicted in Fig. 1 (first row);
(b) a Digital_Controller which currently is a first-order pole-zero compensator and is to be replaced by advanced control algorithms;
(c) a Position_Sensor which is a device that detects the mirror position and converts it into the electrical signal supplied to the controller;
(d) the Scanner_Dynamics block which incorporates the dynamic model of the scanner.

The scanner dynamics block is presented in more detail in Fig. 3. It consists of the following:

(a) a Power_Amplifier block which includes the linear amplifier acting on the difference between the current demand from the controller and the actual motor current; the amplifier interface block limits the controller signal;
(b) the Mechanism which is the main part of the model and consists of the Actuator and the representation for the Scanner_Load, as seen in Fig. 4.

The inputs to the Actuator are the motor command signal V_m from the Power_Amplifier, the motor position θ_1 (rad/s) and the motor speed $\dot{\theta}_1$. The motor current i_m is described by the first-order transfer function:

$$i_m = (sL + R)^{-1} \Delta V \tag{1}$$

where ΔV represents the voltage supplied to the motor and is described by the equation

$$\Delta V = V_m - \dot{\theta}_1 p_f K_b \tag{2}$$

In equation (2), V_m is the motor command (the signal from the power amplifier).

Finally, the electric torque, which is the output of the Actuator and the input to the Scanner_Load is expressed by the equation

$$T_e = i_m p_f K_t - c_g \tag{3}$$

Two coefficients in the torque equation represent non-linear effects in the actuator. These are the profile p_f and cogging c_g. Both the profile and the cogging are functions of the motor position. L, R, K_b and K_t are constant parameters.

The load block represents a second-order dynamics of the motor given by

$$\ddot{\theta}_1 = \frac{T_o - T_t}{J_1} \tag{4}$$

and the second-order dynamics of the mirror given by

$$\ddot{\theta}_2 = \frac{T_t}{J_2} \tag{5}$$

These two are linked by the torsional effect equation:

$$T_t = K_t(\theta_1 - \theta_2) \tag{6}$$

where θ_1 is the motor angle (rad), θ_2 is the mirror angle (rad), and J_1 and J_2 represent the motor and the mirror moments of inertia (kg m^2) respectively. The output torque T_o is a non-linear function of the electric torque T_e and the friction. Friction and stiction are both included in the friction model.

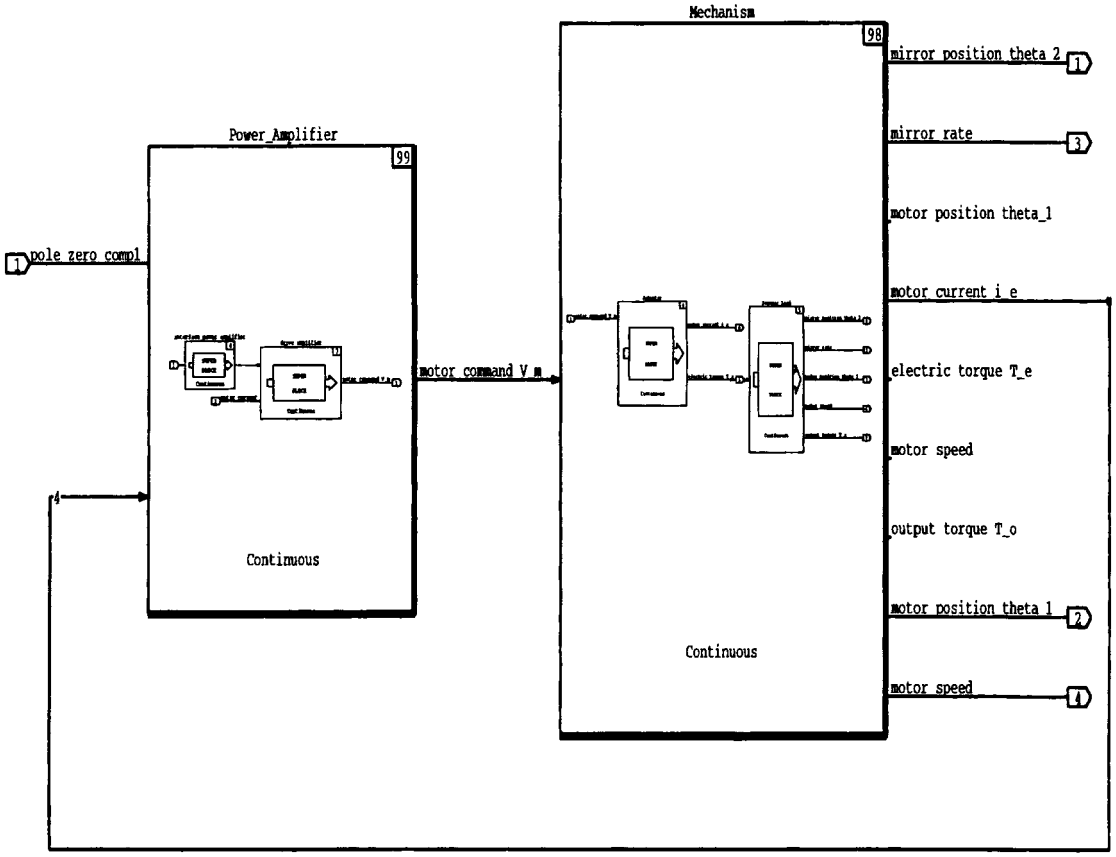

Fig. 3 The scanner dynamics

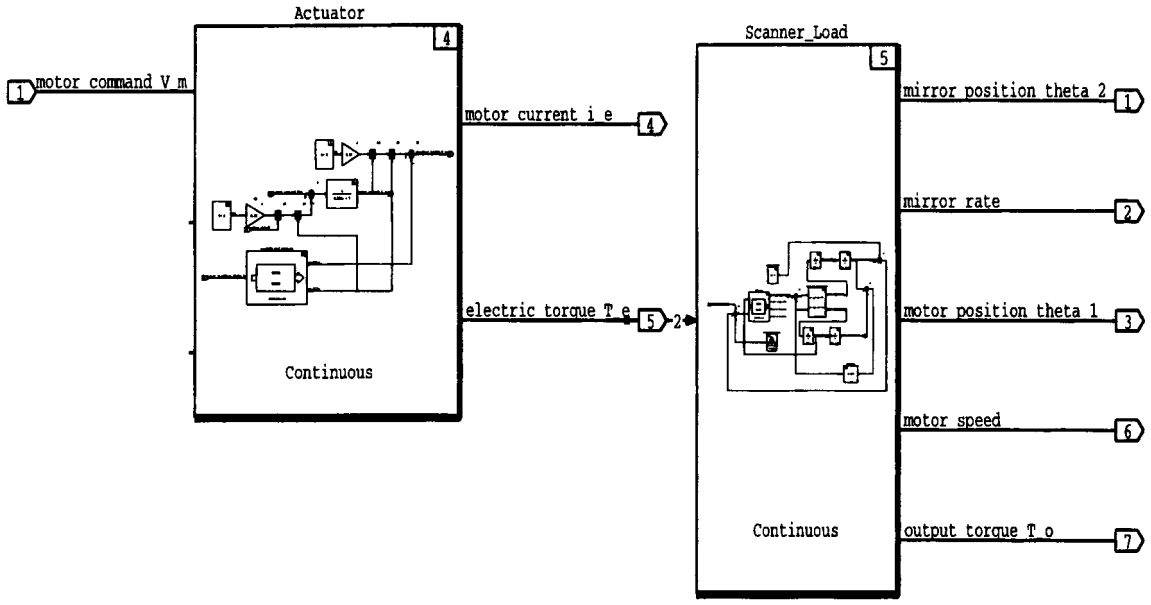

Fig. 4 The scanner mechanism

3 ADVANCED CONTROLLER DESIGN AND COMPARISONS

3.1 Existing compensator

The pole-zero compensator currently implemented in the scanner system is a first-order digital controller described by the equation

$$u_t = (b_1 z - b_2)^{-1}(a_1 z - a_2)(r_t - y_t) \tag{7}$$

where u_t is the control signal (current demand), i.e. the output signal from the Digital_Controller in Fig. 2), r_t is the reference signal, i.e. the output signal from the Ramp_Generator in Fig. 2, and y_t is the position feedback signal, i.e. the output signal from the Position_Sensor in Fig. 2. The controller works with a sampling frequency of 16 kHz.

3.2 H_∞ control

3.2.1 Introduction to H_∞ control theory

The design of H_∞ controllers is based on an optimization which gives an equalized frequency response. Of course, equalizing is not a desirable closed-loop property of a control system. The remedy which makes an equalizing optimization useful and powerful in control design is known as the *standard problem concept.*

In the standard problem, depicted in Fig. 5, $\mathbf{G}(s)$ is an abstract transfer matrix with two vector inputs $\boldsymbol{w}$ and $\boldsymbol{u}$ and two vector outputs $\boldsymbol{z}$ and $\boldsymbol{y}$. $\mathbf{G}(s)$ will typically contain the plant model, but it will never be *just* the plant model. The actual contents of $\mathbf{G}(s)$ depend heavily on the type of control problem which H_∞ optimization is applied to. It will always contain weightings, which are

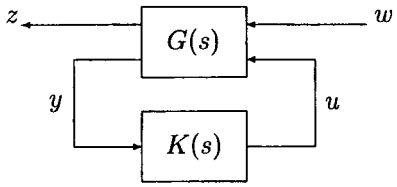

Fig. 5 The H_∞ standard problem

the reciprocals of the desired loop shapes. In the optimization then the required loop shape is obtained by equalizing the combination of the plant and the weightings. Furthermore, in a typical H_∞ design, $\mathbf{G}(s)$ will include uncertainty models, noise models and disturbance models. $\boldsymbol{w}$ can be interpreted as an undesired exogenous signal, $\boldsymbol{u}$ is the control action, $\boldsymbol{y}$ contains the measurements and $\boldsymbol{z}$ is an error signal that should be kept as small as possible.

Once a standard problem in the form of Fig. 5 is defined, the controller $\mathbf{K}(s)$ is computed using H_∞ optimization. H_∞ optimization amounts to the solution of two algebraic Riccati equations [**5**]. The optimization will typically include a linear search by introducing a scalar parameter in the weightings. For a thorough introduction to H_∞ theory including the recipes for setting up standard problems, see reference [**2**].

The approach taken for the scanner system was a two-degrees of freedom (TDOF) design formulated in a standard problem set-up as a tracking problem with a reference model. Descriptions of TDOF designs can be found in numerous references (see, for example, references [**6**] and [**7**]).

3.2.2 Reformulating the design specifications

Since H_∞ is in essence a frequency domain technique, time domain specifications have to be recast as frequency

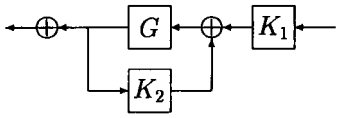

Fig. 6 TDOF architecture: K_1 is the feedforward controller and K_2 is the feedback controller

domain specifications. In the present case, this meant that the L_∞ specification for the tracking error had to be transformed into a bandwidth specification for the transfer function from reference signal to tracking error. There is no one-to-one correspondence between L_∞ and bandwidth specifications, but a reasonable approach is to apply Fourier analysis to the reference signal and to require the bandwidth to include at least those harmonics that have amplitudes larger than or comparable with the maximally allowable error amplitude. In the present case, the bandwidth required using this approach was 1000 rad/s. This method turned out to work quite well for the scanner design.

3.2.3 H_∞ controller architecture

The laser scanner model was characterized by the following properties: strong non-linearities, dominant oscillatory unstable modes and an infinite zero structure. This calls for stability and performance issues to be addressed independently in order for the design to be robust. For this reason a TDOF architecture was chosen with a feedforward and a feedback block as shown in Fig. 6.

The purpose of the feedback controller is to stabilize the system and to provide as much bandwidth as is allowed by the non-linear dynamics without introducing non-minimum phase zeros inside the bandwidth specification, i.e. the feedback controller is not allowed to have unstable poles less than 1000 rad/s. The purpose of the feedforward controller is to provide the remaining bandwidth by amplifying fast components of the reference signal. The application of H_∞ control synthesis in itself does not guarantee robustness. Robustness in general is obtained only if designed for and can be achieved using techniques other than H_∞. In this case study, for comparison with the other methods, it was chosen not to make a robust design. In fact, the final design turned out to be reasonably robust with respect to parametric uncertainties, but that was related more to the zero structure of the plant than to the applied methods (parameter robustness is easier to obtain for a plant having no finite zeros).

3.2.4 H_∞ standard problem set-up and weight selection

To derive a standard problem set-up from the architecture in Fig. 6, the following are required:

1. Weightings should be introduced.
2. 'Disturbance' signals must be defined.
3. 'To-be-controlled' outputs must be identified.

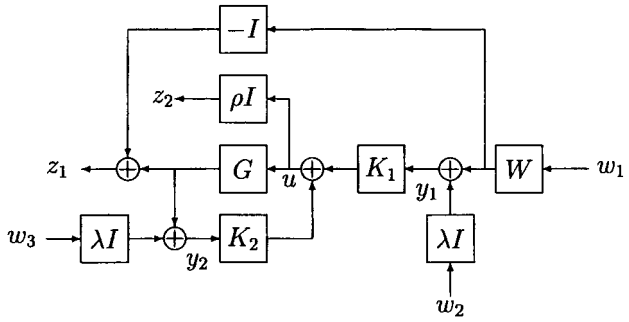

Fig. 7 Standard problem set-up

1. The most important weighting was of course the reference model, which is also well justified since the reference signal was known in advance. For the architecture selected, it could also be relevant to have weightings representing actuator and sensor models, and possibly a noise model. However, these effects seemed to play minor roles; therefore only the reference weighting was included in the final design in order to keep the controller order down.
2. When introducing a weighting in front of the physical reference signal, the generating signal w_1 for the reference signal becomes the exogenous input. In addition to this signal, two fictitious noise signals w_2 and w_3 are added to the two measurement signals in order to prevent too large observer gains.
3. The output to be controlled is the difference between the desired output and the actual output, i.e. the tracking error. In addition to this signal z_1 a constant times the control signal $\boldsymbol{u}$ was introduced as the penalty signal z_2 to prohibit too large feedback gains. The resulting standard problem is depicted in Fig. 7.

The weighting function had to be chosen as a low-pass filter with roll-off at 1000 rad/s. However, since the controller had to be implemented as a sampled data controller with a sampling frequency of 100 000 rad/s, care had to be taken that the control gain would not be extremely high at that sampling frequency. This meant that the weighting function had to roll off at least with 60 dB/decade, since the scanner system itself had a pole excess of five. Eventually, these considerations led to the selection of the weighting as a third-order Bessel filter with a Bessel angular frequency equal to 1000 rad/s. The transfer function in Fig. 7 from $\boldsymbol{w} = (w_1 \ w_2 \ w_3)^{\mathrm{T}}$ to $\boldsymbol{z} = (z_1 \ z_2)^{\mathrm{T}}$ is a linear fractional transformation with respect to the controller:

$$\boldsymbol{u}(s) = [K_1(s) \quad K_2(s)] \begin{pmatrix} y_1 \\ y_2 \end{pmatrix} \tag{8}$$

where $K_1(s)$ is the feedforward controller and $K_2(s)$ is the feedback controller in the following open-loop standard problem configuration:

$$\begin{pmatrix} \dot{x} \\ \dot{x}_W \end{pmatrix} = \begin{pmatrix} \mathbf{A} & 0 \\ 0 & \mathbf{A}_W \end{pmatrix} \begin{pmatrix} x \\ x_W \end{pmatrix} + \begin{pmatrix} 0 & 0 & 0 \\ \mathbf{B}_W & 0 & 0 \end{pmatrix} \begin{pmatrix} w_1 \\ w_2 \\ w_3 \end{pmatrix} + \begin{pmatrix} \mathbf{B} \\ 0 \end{pmatrix} \boldsymbol{u}$$

$$\begin{pmatrix} z_1 \\ z_2 \end{pmatrix} = \begin{pmatrix} \mathbf{C} & -\mathbf{C}_W \\ 0 & 0 \end{pmatrix} \begin{pmatrix} x \\ x_W \end{pmatrix} + \begin{pmatrix} -\mathbf{D}_W & 0 & 0 \\ 0 & 0 & 0 \end{pmatrix} \begin{pmatrix} w_1 \\ w_2 \\ w_3 \end{pmatrix} + \begin{pmatrix} \mathbf{D} \\ \rho\mathbf{I} \end{pmatrix} \boldsymbol{u}$$

$$\begin{pmatrix} y_1 \\ y_2 \end{pmatrix} = \begin{pmatrix} 0 & \mathbf{C}_W \\ \mathbf{C} & 0 \end{pmatrix} \begin{pmatrix} x \\ x_W \end{pmatrix} + \begin{pmatrix} \mathbf{D}_W & \lambda\mathbf{I} & 0 \\ 0 & 0 & \lambda\mathbf{I} \end{pmatrix} \begin{pmatrix} w_1 \\ w_2 \\ w_3 \end{pmatrix} + \begin{pmatrix} 0 \\ \mathbf{D} \end{pmatrix} \boldsymbol{u} \tag{9}$$

Here,

$$\mathbf{G}(s) = \left(\begin{array}{c|c} \mathbf{A} & \mathbf{B} \\ \hline \mathbf{C} & \mathbf{D} \end{array}\right) \quad \text{and} \quad \mathbf{W}(s) = \left(\begin{array}{c|c} \mathbf{A}_W & \mathbf{B}_W \\ \hline \mathbf{C}_W & \mathbf{D}_W \end{array}\right)$$

are the plant and weighting transfer functions respectively, while ρ and λ are scalar parameters with the dual purpose of regularizing the plant as required for toolbox computations and of controlling filtering and feedback gains as mentioned above.

3.2.5 *Computing the H_∞ controller*

Two commercial toolboxes offer H_∞ optimization, namely the Robust Control Toolbox and the μ-tools toolbox. Both toolboxes are available for both MATLAB and for MATRIXx.

Neither of these two toolboxes was useful without some customization. Entering the data in the model described in Section 2 directly did not result in any controllers. The reason for this was that both toolboxes regarded the system to be non-stabilizable for numerical reasons whereas, on closer examination, the model really turned out to be controllable for structural reasons. The reason for these problems was not obvious since the model seemed quite 'innocent'. A partial explanation is probably that the system had a strongly non-collocated actuator–sensor structure. This tends to generate systems with very ill-conditioned controllability matrices.

As a means of overcoming these numerical problems, a numerically balanced version of the model was computed. However, since the built-in balancing tools broke down (because the system was not well balanced) an *ad hoc* procedure was established, on the basis of geometric methods (the details are omitted due to space limitations). This balanced model was further reduced from a fifth-order model to a fourth-order model in order to bound the resulting controller order. The toolbox methods will always generate controllers with the order of the plant plus that of the weightings. Low controller orders are a basic virtue for engineering design. However, in the present case study this aspect was not so much required from an implementational point of view, but rather because the simulation tools could not handle high-order controllers. As an example, using the built-in conversion from state space to transfer function representations in MATRIXx meant a qualitative change to the outcome of the simulation, i.e. a change from stability to instability, in spite of the fact that the very same controller was applied.

The next issue addressed was discretization, since the controller would be implemented in a sampled-data realization. Again the built-in default did not work very well. In both MATLAB and MATRIXx, the default choice is the Tustin approximation. For the H_∞ controller the Tustin approximation worked at low frequencies only. This meant that the resulting controller was not even stabilizing. Instead, after some trials, the discretization was carried out using the prewarp algorithm, which is based on a bilinear transform, using one-fifth of the sampling frequency for the prewarp.

Following this algorithm, an H_∞ controller was derived which worked quite well for the linearized model. The error signal, i.e. the difference between the command signal and the output of the linearized model using the sampled-data TDOF H_∞ controller, is shown in Fig. 8.

When this TDOF controller was applied to the non-linear model, it did not work very well. It managed to stabilize the non-linear model, but it had a very poor performance. From the simulations it was very clear what happened; each time that the mirror turned its direction, it became stuck because of the static friction. The solution was obvious as well; the low-frequency gains had to be increased. However, this could not easily be built into the design procedure. An inverting-the-plant procedure, which would yield the largest gain producable by the toolbox, would still be a factor of 10^3 too low. Introducing a robust stability/nominal performance (mixed sensitivity) concept would actually have made everything worse (smaller low-frequency gains). On the other hand, trying to work with alternative linearized models obtained by linearizing near the stiction phenomena would also not work, since the high-frequency components would disappear.

An *ad hoc* approach was taken by introducing the low-frequency high gains manually, simply by adding a first-order high-gain low-pass transfer function to the feedback part of the controller. This immediately overcame the problem, and the design specifications were met in the first iteration. The result of this design can be seen in Fig. 9, which compares the resulting error from the existing pole-zero compensator with the TDOF H_∞ controller. Note that the error from the

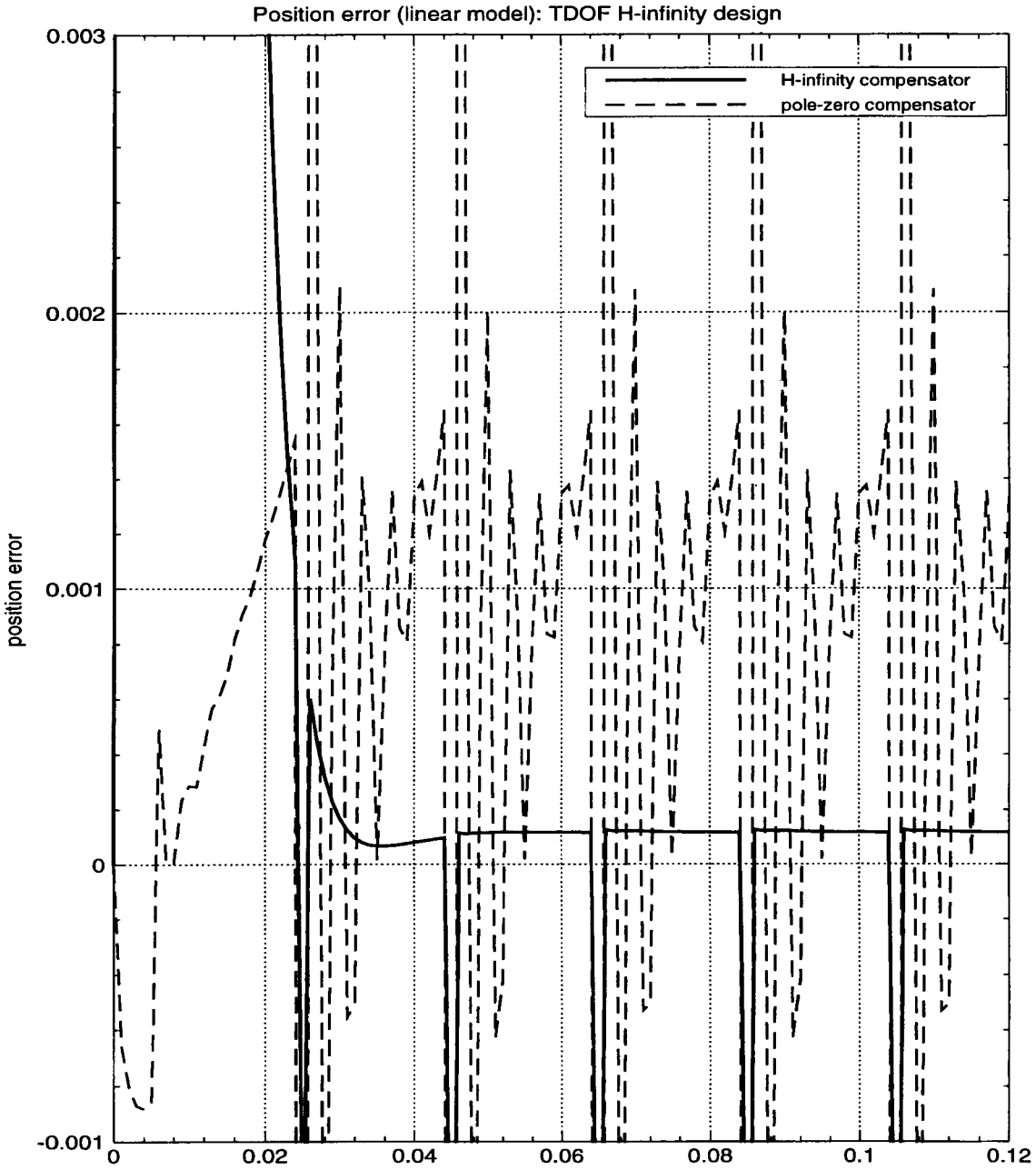

Fig. 8 TDOF H_∞ controller for the linearized model. The vertical axis shows the tracking error in radians and the horizontal axis the time in seconds

controller does not have high-frequency oscillations. If the boundaries of the allowable tracking error are set as (0.0005, 0.001) (rad), the actual tracking error stays well within the boundaries during 85 per cent of each period. The resulting controller was of the same order as the standard problem, i.e. its state space has $5-1=4$ dimensions from the reduced order model, three dimensions from the Bessel filter, one dimension from the first-order low-pass gain; therefore the total controller order was eight. With some effort this could be reduced a little, but not substantially.

3.3 Generalized predictive control

3.3.1 Introduction to the algorithm

The design of predictive control algorithm requires some initial manipulations on the scanner system model. Firstly, the existing non-linear model of the scanner must be linearized around the operating point. This has been performed using a standard MATRIXx function. Secondly, the resulting model, which is expressed in continuous time, must be discretized, as the generalized predictive controller utilizes a discrete time model. Several

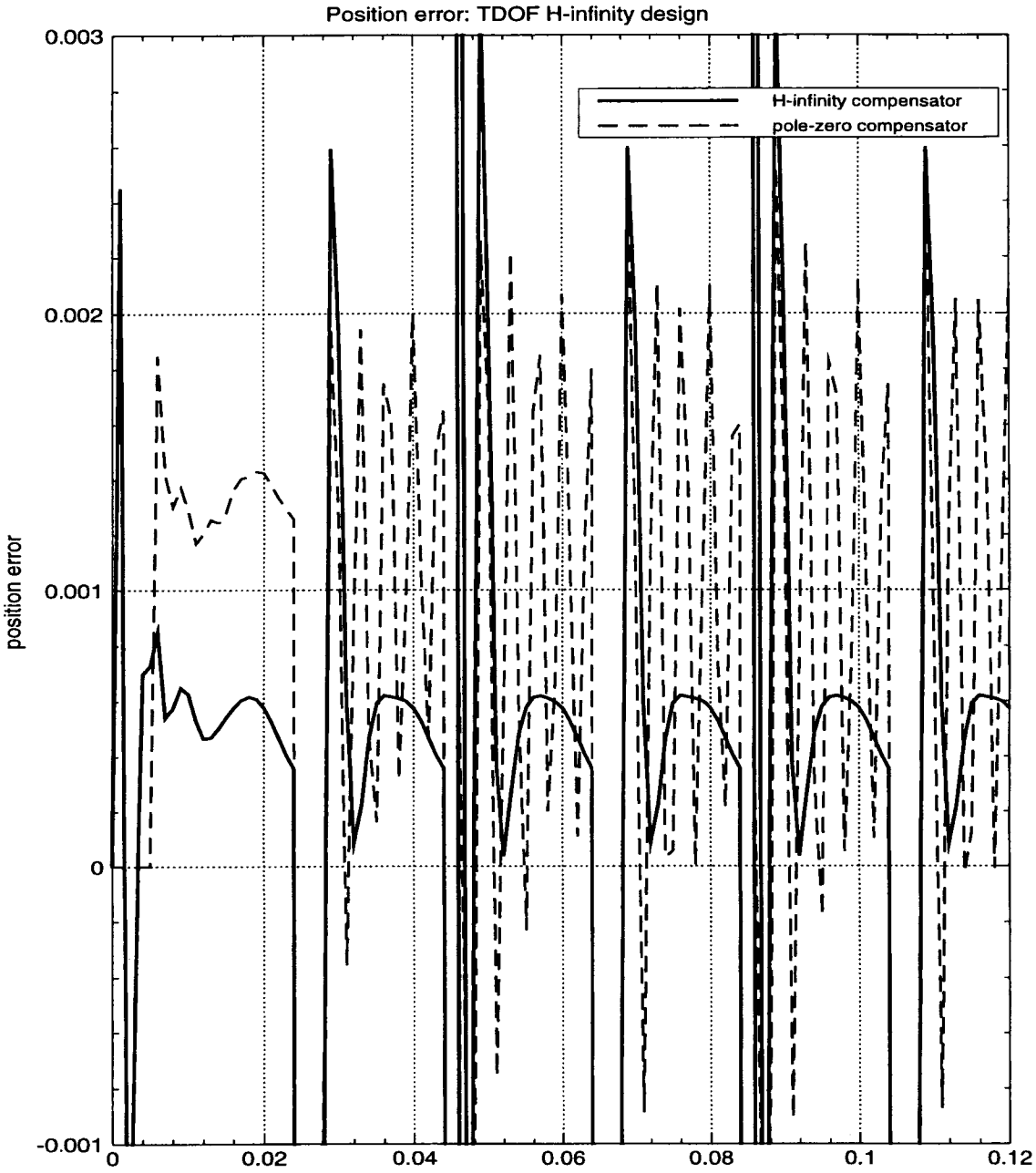

Fig. 9 TDOF H_∞ controller for the non-linear model. The vertical axis shows the tracking error in radians and the horizontal axis the time in seconds

methods of discretization are available in MATRIXx. Some of these, e.g. the impulse invariant transformation, lead to numerical difficulties in the subsequent controller design. Finally, the trapezoidal (Tustin) method was selected as one of the simplest which will do the job. When applying the Tustin discretization, due to its trapezoidal character, the resulting discrete time model usually has direct-through terms, i.e. algebraic connections between input and output signals. Some of the complex dynamic blocks (superblocks) in the scanner model do exhibit direct-through terms, mainly due to the representation of non-linear effects of profile and cogging, and therefore the Tustin method is consistent with other operations performed on discrete superblocks within the package. However, the generalized predictive control (GPC) algorithm must be modified to handle this situation.

After linearization and discretization the system considered is described by linear discrete time state space equations in the form

$$\begin{aligned} \boldsymbol{x}_{t+1} &= \mathbf{A}\boldsymbol{x}_t + \mathbf{B}\boldsymbol{u}_t \\ y_t &= \mathbf{C}\boldsymbol{x}_t + \mathbf{D}\boldsymbol{u}_t \end{aligned} \tag{10}$$

where

$\boldsymbol{x}_t$ = vector of state variables
$\boldsymbol{u}_t$ = vector of inputs which are manipulated control signals
$\boldsymbol{y}_t$ = vector of output variables
$\mathbf{A}$, $\mathbf{B}$, $\mathbf{C}$, $\mathbf{D}$ = constant matrices ($\mathbf{D}$ defines the direct through terms)

In order to simplify the derivation of the optimal control and to eliminate the direct-through terms it is mathematically convenient to rearrange the state equations (10), by extending the state vector to include the control signals as follows:

$$\boldsymbol{\chi}_{t+1} = \tilde{\mathbf{A}}\boldsymbol{\chi}_t + \tilde{\mathbf{B}}\,\Delta\boldsymbol{u}_{t+1} \tag{11}$$

$$\boldsymbol{y}_t = \tilde{\mathbf{C}}\boldsymbol{\chi}_t \tag{12}$$

where

$$\boldsymbol{\chi}_t = \begin{pmatrix} x_t \\ u_t \end{pmatrix} \tag{13}$$

$$\Delta\boldsymbol{u}_{t+1} = \boldsymbol{u}_{t+1} - \boldsymbol{u}_t \tag{14}$$

$$\tilde{\mathbf{A}} = \begin{pmatrix} \mathbf{A} & \mathbf{B} \\ 0 & \mathbf{I} \end{pmatrix}, \qquad \tilde{\mathbf{B}} = \begin{pmatrix} 0 \\ \mathbf{I} \end{pmatrix}, \qquad \tilde{\mathbf{C}} = (\mathbf{C} \quad \mathbf{D}) \tag{15}$$

Having obtained the extended state equations of the system, the derivation of the generalized predictive controller can be performed as in a standard case. The k-step-ahead output prediction becomes

$$\begin{aligned} \boldsymbol{y}_{t+k} &= \tilde{\mathbf{C}}\boldsymbol{\chi}_{t+k} \\ &= \tilde{\mathbf{C}}\tilde{\mathbf{A}}^k\boldsymbol{\chi}_t + \sum_{j=1}^{k} \tilde{\mathbf{C}}\tilde{\mathbf{A}}^{k-j}\tilde{\mathbf{B}}\,\Delta\boldsymbol{u}_{t+j} \end{aligned} \tag{16}$$

If the prediction is performed for different time horizons (from N_1 to N_2), the result may be collected in a block vector $\boldsymbol{Y}_{t,N_1,N_2}$:

$$\boldsymbol{Y}_{t,N_1,N_2} = \begin{pmatrix} \boldsymbol{y}_{t+N_1} \\ \mathbf{y}_{t+N_1+1} \\ \vdots \\ \boldsymbol{y}_{t+N_2} \end{pmatrix} \tag{17}$$

Consequently, the prediction equations, when k changes from N_1 to N_2 can be written in a vector form as follows:

$$\boldsymbol{Y}_{t,N_1,N_2} = \boldsymbol{\Phi}_{N_1,N_2}\boldsymbol{\chi}_t + \mathbf{G}_{N_1,N_2}\boldsymbol{U}_{t,N_2} \tag{18}$$

where

$$\boldsymbol{\Phi}_{N_1,N_2} = \begin{pmatrix} \tilde{\mathbf{C}}\tilde{\mathbf{A}}^{N_1} \\ \tilde{\mathbf{C}}\tilde{\mathbf{A}}^{N_1+1} \\ \vdots \\ \tilde{\mathbf{C}}\tilde{\mathbf{A}}^{N_2} \end{pmatrix} \tag{19}$$

$$\mathbf{G}_{N_1,N_2} = \begin{pmatrix} \tilde{\mathbf{C}}\tilde{\mathbf{A}}^{N_1-1}\tilde{\mathbf{B}} & \tilde{\mathbf{C}}\tilde{\mathbf{A}}^{N_1}\tilde{\mathbf{B}} & & & \\ \tilde{\mathbf{C}}\tilde{\mathbf{A}}^{N_1-2}\tilde{\mathbf{B}} & \tilde{\mathbf{C}}\tilde{\mathbf{A}}^{N_1-1}\tilde{\mathbf{B}} & & \mathbf{0} & \\ \vdots & \vdots & & & \\ \tilde{\mathbf{C}}\tilde{\mathbf{A}}^{N_2-1}\tilde{\mathbf{B}} & \tilde{\mathbf{C}}\tilde{\mathbf{A}}^{N_2-2}\tilde{\mathbf{B}} & \cdots & \tilde{\mathbf{C}}\tilde{\mathbf{A}}\tilde{\mathbf{B}} & \tilde{\mathbf{C}}\tilde{\mathbf{B}} \end{pmatrix} \tag{20}$$

$$\boldsymbol{U}_{t,N_2} = \begin{pmatrix} \Delta\boldsymbol{u}_{t+1} \\ \Delta\boldsymbol{u}_{t+2} \\ \vdots \\ \Delta\boldsymbol{u}_{t+N_2} \end{pmatrix} \tag{21}$$

In addition, it should be noted that the signals $\Delta\boldsymbol{u}_{t+j}$ are in fact the changes in the control signal [see equation (14)]. Therefore, it is justified to assume that the signal $\Delta\boldsymbol{u}_{t+j}$ will become zero after a few sampling intervals into the future, i.e. no changes in the control signal are envisaged in the remote future. The non-zero control actions can be combined in a vector:

$$\boldsymbol{U}_{t,N_u} = \begin{pmatrix} \Delta\boldsymbol{u}_{t+1} \\ \Delta\boldsymbol{u}_{t+2} \\ \vdots \\ \Delta\boldsymbol{u}_{t+N_u} \end{pmatrix} \tag{22}$$

As seen from the above equations, the dimensions of the $\mathbf{G}_{N_1,N_2}$ matrix are reduced by setting a control horizon $N_u < N_2$. After N_u steps into the future the control increment is set to zero. Thus the last $N_2 - N_u$ rows of $\mathbf{G}_{N_1,N_2}$ may be deleted, since in this case they make no contribution to the output prediction. N_u represents a tuning parameter in GPC, which may be used to shape the control performance and to stabilize non-minimum phase or unstable plants.

The performance index is then defined as follows:

$$J_t = \sum_{j=N_1}^{N_2} (\boldsymbol{y}_{t+j} - \boldsymbol{r}_{t+j})^2 + \lambda \sum_{j=1}^{N_u} \Delta\boldsymbol{u}_{t+j} \tag{23}$$

When the system variables are unconstrained there exists an analytical solution of the problem [**8**]. Substituting equation (18) and minimizing with respect to $\boldsymbol{U}_{t,N_u}$ yields

$$\begin{aligned} \boldsymbol{U}^{\text{opt}}_{t,N_u} = (\mathbf{G}^{\mathrm{T}}_{N_1,N_2,N_u}\mathbf{G}_{N_1,N_2,N_u} + \lambda\mathbf{I})^{-1}\mathbf{G}^{\mathrm{T}}_{N_1,N_2,N_u} \\ \times (\boldsymbol{R}_{t,N} - \boldsymbol{\Phi}_{N_1,N_2}\tilde{\mathbf{A}}\boldsymbol{\chi}_t) \end{aligned} \tag{24}$$

where

$\boldsymbol{R}_{t,N}$ = vector of the future values of the reference signal

Because a receding horizon strategy is employed, only the first element of the predicted optimal controls vector $\boldsymbol{U}_{t,N_u}$ is actually applied to the system. At each sampling instance, new measurement information becomes available and $\boldsymbol{U}_{t,N_u}$ is updated according to equations (11) and (24). If the future reference signal matches exactly the predicted free response summed with a known future disturbance component, then the current control increment will be zero.

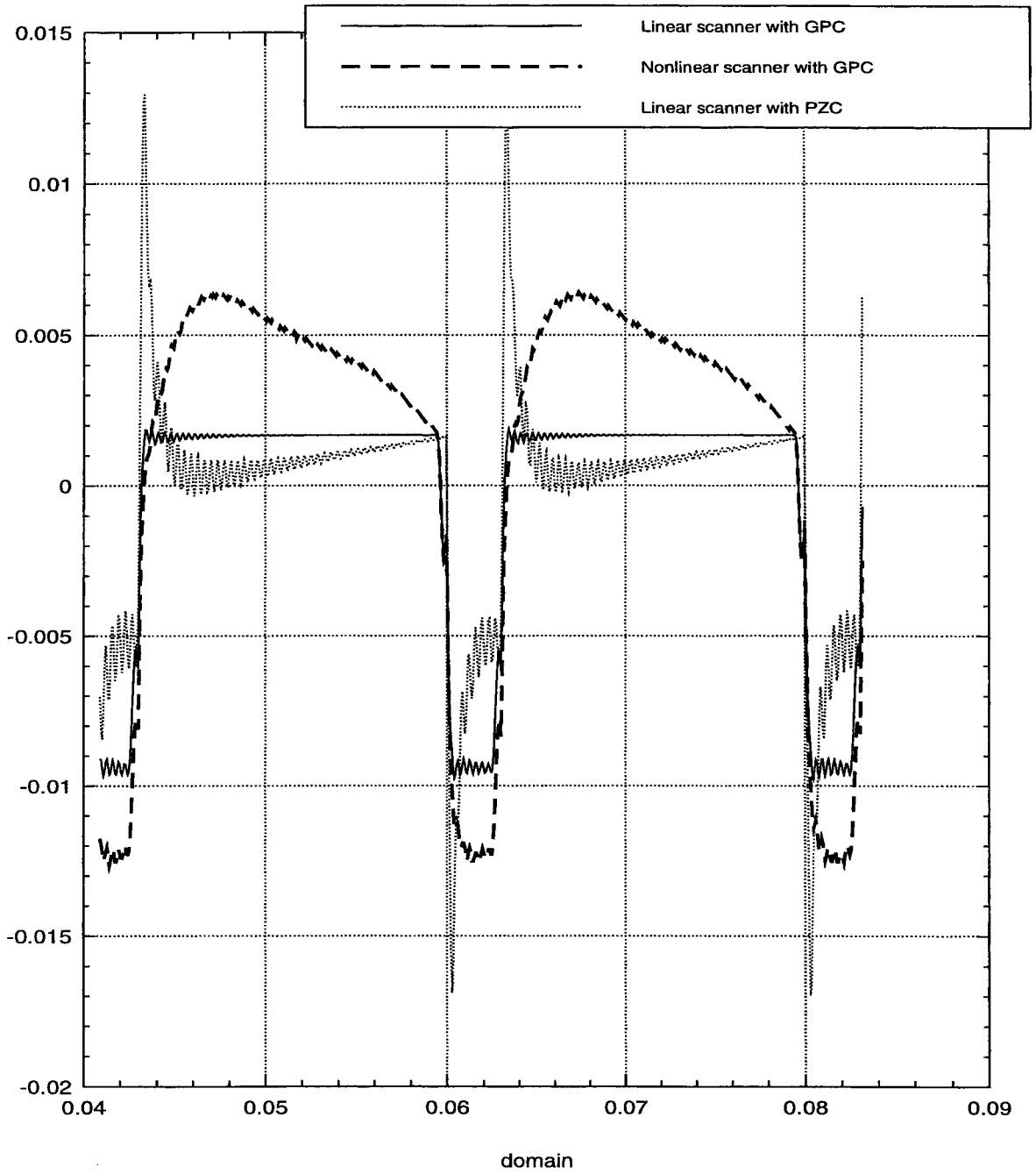

Fig. 10 Comparison of scanning errors for a generalized predictive controller (GPC) with a linear scanner model, for a pole-zero compensator (PZC) with a linear scanner model and for a GPC with a non-linear scanner model. The vertical axis shows the tracking error in radians and the horizontal axis the time in seconds

3.3.2 Implementation of GPC

The algorithm described in the previous section has been tested on the non-linear scanner model. This appeared to be a difficult task.

Firstly, the linearized version of the scanner model, which has been utilized in the predictive control design is unstable. The predictive controller must stabilize the system. Note that the generalized predictive controller presented in this paper is capable of stabilizing an unstable scanner model. This is not an obvious feature of all predictive controllers.

Secondly, an interesting feature of the analysed model is that it requires a vigorous control action for stabilization. Even a minimal costing on control signals in the performance index causes instability of the whole system.

Thirdly, a large increase in the output tracking horizon is not beneficial to the system performance. This is prob-

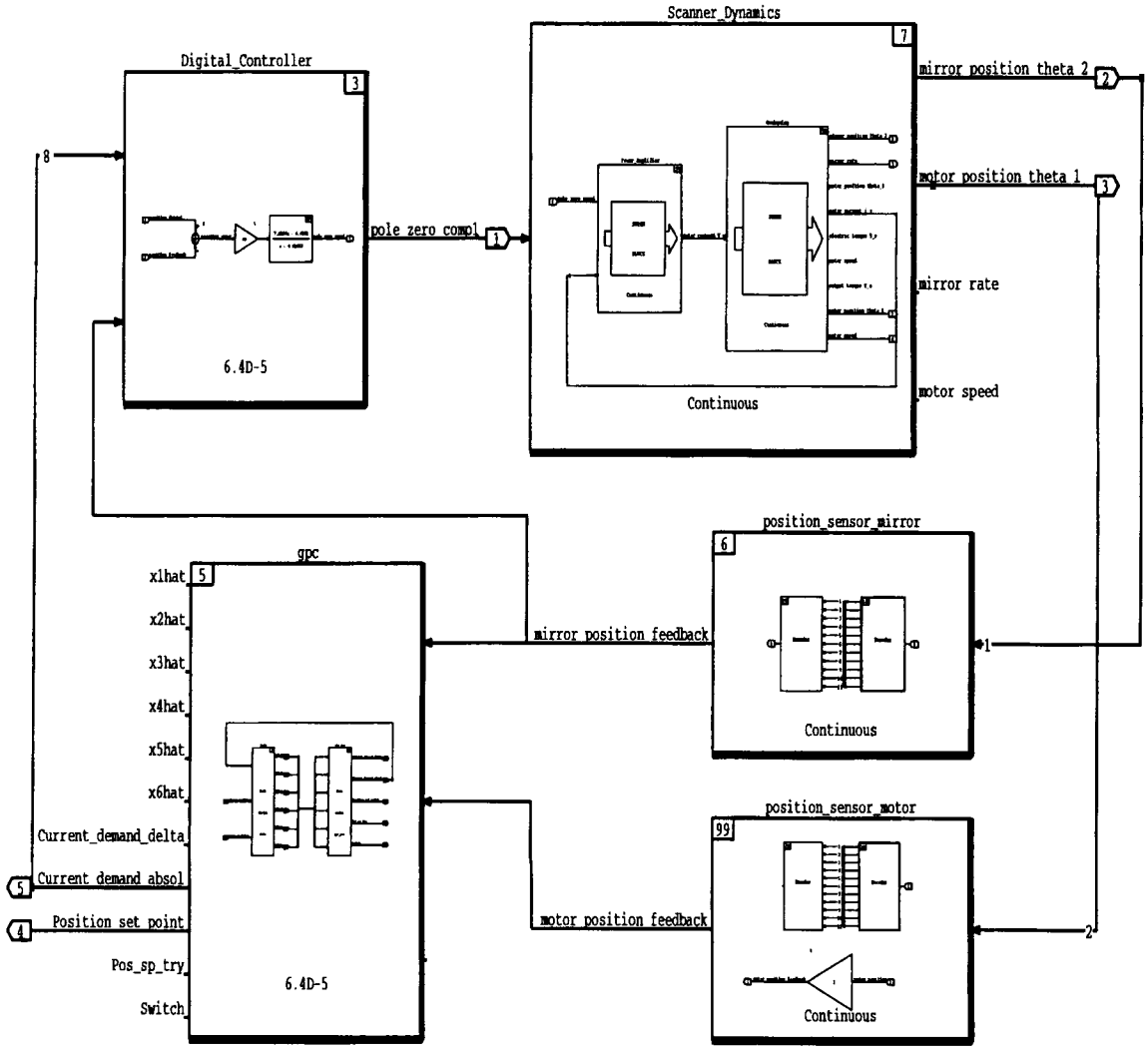

Fig. 11 The cascade structure for predictive control

ably because the second part of the reference signal, the mirror return part, is very fast and therefore difficult to follow. In fact, a tight tracking of the reference is not required for this part. Nevertheless, GPC tries to minimize the error also for the mirror return part of the reference signal. This can be detrimental to the overall performance, especially for long tracking horizons.

The tuning parameters for the generalized predictive controller have been selected, taking into account the above considerations. The best results were achieved for the following settings (the sampling frequency is 16 kHz): $N_1 = 1$, $N_2 = 12$, $N_u = 1$ and $\lambda = 0$. The results of applying GPC to the linear scanner model are shown in Fig. 10. In comparison with the pole-zero compensator applied to the same linear model, the generalized predictive controller performs much better. The overshoot is eliminated and the error signal remains constant for almost the whole time of the forward movement of the mirror. However, when the same generalized predictive controller was used with the non-linear scanner model the performance deteriorated significantly. In fact, the tuning parameters which were selected as optimal in the linear case were no longer satisfactory. Some additional tuning was required to improve the performance. The new settings for the controller were $N_1 = 1$, $N_2 = 20$, $N_u = 2$ and $\lambda = 0$.

However, even after this additional tuning, the performance achieved was not entirely satisfactory. Replacing the existing pole-zero compensator with a generalized predictive controller resulted in much smaller overshoots at the beginning and at the end of the scanning period. However, the error during the rest of the scanning period was not better than with the pole-zero compensator (see Fig. 10).

Another approach tried in this implementation experiment was to leave the existing pole-zero compensator and to apply a generalized predictive controller in an outer loop, providing set point value for the pole-zero compensator (cascade control, as depicted in Fig. 11). This approach is justified by the fact that the pole-zero compensator provides stabilization of the scanner system. Then the role of GPC would be to optimize the

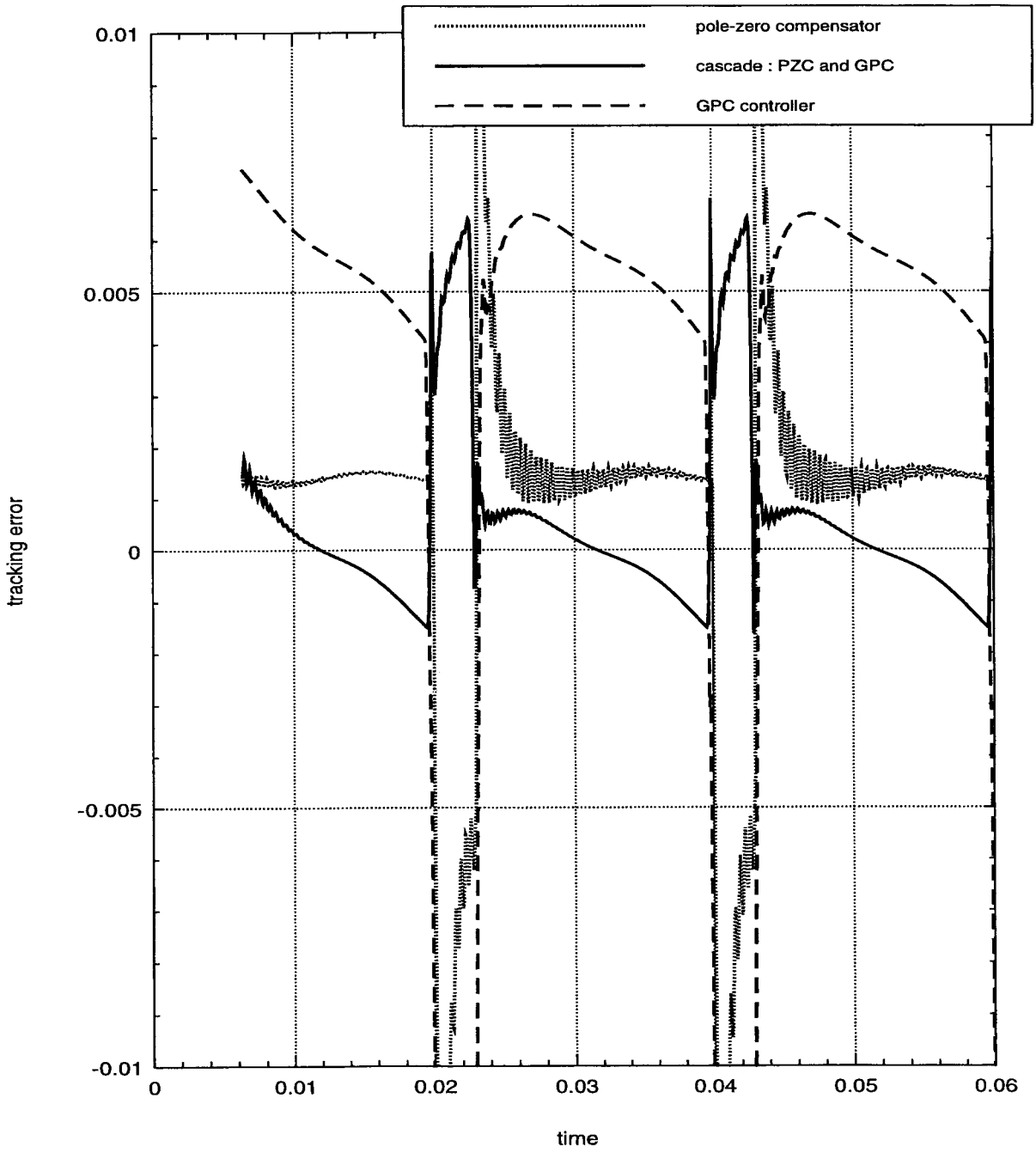

Fig. 12 Comparison of scanning errors for a pole-zero compensator (PZC), for a generalized predictive controller (GPC) and for a cascade of a pole-zero compensator (PZC) and for a GPC, all applied to the non-linear scanner model. The vertical axis shows the tracking error in radians and the horizontal axis the time in seconds

performance. For this exercise the scanner and the pole-zero compensator, in a closed loop, were linearized and discretized together and the resulting model was used in the GPC design. Of course, the linear model used for design would be different from before. In particular, the pole-zero compensator will increase the overall order of the model dynamics by one. The following settings were selected for GPC parameters: $N_1 = 1$, $N_2 = 15$, $N_u = 1$ and $\lambda = 0$.

The results of the above-described experiments are depicted in Fig. 12. It is easy to see that the last of the described approaches provides a superior performance of the system. In both cases of implementation of GPC, the immediate result was the elimination of overshoots at the beginning and at the end of the scanning period. This of course can help to improve the scan efficiency. However, it was difficult to achieve a noticeable reduction in the scanning error. To obtain better results

it would probably be necessary to return to the modelling exercise and to construct a more exact linear model of the scanner.

4 CONCLUSIONS

The paper presents an exercise on feasibility of modern control techniques, namely H_∞ and model-based predictive control, to provide a required performance in the trajectory following problem for the laser scanner system. The scanner system poses serious difficulties to the control design due to its strong non-linearity (caused mainly by the static friction) and the highly undamped instability of the linearized model. Practical design issues associated with the above difficulties are mentioned in the paper. Some of these, e.g. selection of a discretization method appropriate for a given model of the system or selection of a form of the linearized model, have indeed proven to influence the achieved performance of the system. However, a more systematic analysis of these effects was outside the scope of this study.

After some careful tuning, both H_∞ and GPC were capable of successfully controlling the system. Particular features of the compared algorithms are as follows:

1. H_∞ provides a lower value of the scanning error during the linear scanning period than the GPC algorithm.
2. GPC is capable of removing overshoots at the beginning and at the end of the scanning period, which poses difficulties for the H_∞ algorithm.
3. The H_∞ controller was easier to tune than the GPC.

ACKNOWLEDGEMENTS

This paper was originated by a case study project realized by Advanced Control Technology Club, Glasgow for Barr and Stroud Limited.

REFERENCES

1 **Marshall, G. F.** Scanner refinements inspire new users. *Laser Focus World*, June 1994, 2–6.
2 **Zhou, K., Doyle, J. C.** and **Glover, K.** *Robust and Optimal Control*, 1996 (Prentice-Hall, Englewood Cliffs, New Jersey).
3 **Armstrong-Helouvry, B., Dupont, P.** and **Canudas de Wit, C.** A survey of models, analysis tools and compensation methods for the control of machines with friction. *Automatica*, 1994, **30**(7), 1083–1138.
4 **Canudas de Wit, C., Olsson, H., Åström, K. J.** and **Lischinsky, P.** A new model for control of systems with friction. *IEEE Trans. Autom. Control*, March 1995, **40**(3), 419–425.
5 **Doyle, J., Glover, K., Khargonekar, P.** and **Francis, B. A.** State-space solutions to standard H_2 and H_∞ control problems. *IEEE Trans. Autom. Control*, 1989, **34**, 831–847.
6 **Limebeer, D. J. N., Kasenally, E. M.** and **Perkins, J. D.** On the design of robust two degrees of freedom controllers. *Automatica*, 1993, **29**(1), 157–168.
7 **Grimble, M. J.** Minimization of a combined H_∞ and LQG cost function for a two-degrees-of-freedom control design. *Automatica*, 1989, **25**(4), 635–638.
8 **Ordys, A. W.** and **Clarke, D. W.** A state-space description of GPC controllers. *Int. J. Syst. Sci.*, 1993, **23**(2), 1727–1744.